Supplementary Material for

Bio-inspired Synergistic Wing and Tail Morphing Extends Flight Capabilities of Drones

E. Ajanic[*], M. Feroskhan, S. Mintchev, F.Noca, D. Floreano[*]

*Corresponding authors: {enrico.ajanic, dario.floreano}@epfl.ch

This PDF file includes:

Supplementary Material

Wing Airfoil Selection. The flying wing design posed challenges in the airfoil selection process. Conventional aircraft achieve balanced flight in longitudinal direction through their horizontal tail (*5*). When conceptualizing the LisHawk, we had to select airfoils, which permitted balanced flight without horizontal stabilizer to allow a shift from a positive pitch stability to negative pitch stability. During this airfoil design process, we used XFLR5 (vortex lattice method) to evaluate relevant stability and balance characteristics of the entire wing. As seen in Fig. S1, the inner, the center and the outer section can be distinguished:

The feathered outer section resembles a flat plate due to the flat nature of the artificial feathers used for the morphing. Hence, this section was modelled as a flat plate. Then, the center section had to accommodate the wrist cage and the wrist flexing mechanism. While avian airfoils would have induced a large negative pitching moment (birds use a large washout angle to compensate), we adapted the eagle airfoil from (56) by reducing the camber to 1.5%. No airfoil data for the northern goshawk wing was available. The camber adaption was necessary to limit the negative pitching moment inherent in positively cambered airfoil. Last, for the inner wing to counterbalance the negative pitching moment and to achieve balanced flight, we chose the JWL-065 airfoil with a reflex trailing edge.

Finally, the used airfoils for the LisHawk wing (Fig. S2A) diverge significantly from the avian counterpart (Fig. S1B). This is due to design restrictions of the LIS Hawk robot. Large undercambered airfoils would not have sufficed for housing the folding mechanism and the lack of wing twisting would not have allowed achieving balanced flight (17).

Derivation of Linear Acceleration in the Wind Axis. The linear accelerations acting on the aircraft's center of gravity in the wind frame (wf, see Fig. S2) with the basis vectors $\vec{e}_x$, $\vec{e}_y$, and $\vec{e}_z$ can be defined as

$$\vec{a}_{wf} = \underbrace{\dot{V}}_{=a_{wf,x}} \vec{e}_x + \underbrace{\dot{\psi} V cos\gamma}_{=a_{wf,y}} \vec{e}_y + \underbrace{\dot{\gamma} V}_{=a_{wf,z}} \vec{e}_z, \tag{1}$$

with $\dot{V}$ being the change in path velocity of the aircraft, $\dot{\psi}$ being the change in path azimuth angle in the lateral plane, and $\dot{\gamma}$ being the change in heading angle in the longitudinal plane (8).

Correspondingly, as commonly done in flight dynamics when analysing the flight path behavior (8), the point-mass model is considered. The relation between the resultant force vector $\vec{F}$ and the acting force vectors, such as thrust $\vec{T}$, lift $\vec{L} = f(C_L, V, S, ...)$, drag $\vec{D} = f(C_D, V, S, ...)$, and weight $\vec{W} = f(m, g, ...)$ can be shown and separated into the wind-fixed components so that

$$\begin{aligned}\vec{F} &= \vec{T} + \vec{L} + \vec{D} + \vec{W} \\ &= (T\,cos\varepsilon - D - W\,sin\gamma)\vec{e}_x \\ &+ (T\,sin\varepsilon + L)sin\phi\,\vec{e}_y \\ &- [(T\,sin\varepsilon + L)\cos\phi - Wcos\gamma]\vec{e}_z.\end{aligned} \tag{2}$$

Here, the angle of climb is denoted with γ, the bank angle with φ, and deviation angle of the thrust with respect to the flight path with ε. Zero sideslip angle is assumed. Combining Eq. 1 and Eq. 2 yields the so-called dynamic equation in the wind-fixed frame based on the point-mass model (11), so that

$$\vec{a}_{wf} = \begin{pmatrix} \dot{V} \\ \dot{\psi} V cos\gamma \\ \dot{\gamma} V \end{pmatrix} = \begin{pmatrix} \dfrac{Tcos\varepsilon - D}{m} - g\,sin\gamma \\ -\dfrac{(T\,sin\varepsilon + L)sin\varphi}{m} \\ \dfrac{(Tsin\varepsilon + L)cos\varphi}{m} - g\,cos\gamma \end{pmatrix} \tag{3}$$

As treated in the introduction, a large thrust force can evidently increase maneuverability, which is seen in Eq. 3. The thrust force affects the acceleration in every wind axis direction, however, the interest of this paper is in the leverage of aerodynamic forces on maneuverability, and hence gliding flight (gl) is assumed with = 0 , which simplifies Eq. 3 so that

$$\vec{a}_{wf,gl} = \begin{pmatrix} \ddot{x}_{wf} \\ \ddot{y}_{wf} \\ \ddot{z}_{wf} \end{pmatrix} = \begin{pmatrix} \dot{V} \\ \dot{\psi} V cos\gamma \\ \dot{\gamma} V \end{pmatrix} = \begin{pmatrix} \dfrac{-D}{m} - g\,sin\gamma \\ -\dfrac{L\,sin\varphi}{m} \\ \dfrac{L\,cos\varphi}{m} - g\,cos\gamma \end{pmatrix} \tag{4}$$

Here, because calm wind conditions are assumed so that $\alpha = \gamma$, Eq. 4 simplifies to

$$\begin{pmatrix} \ddot{x}_{wf} \\ \ddot{y}_{wf} \\ \ddot{z}_{wf} \end{pmatrix} = \begin{pmatrix} \dfrac{-D}{m} - g\,sin\alpha \\ -\dfrac{L\,sin\varphi}{m} \\ \dfrac{L\,cos\varphi}{m} - g\,cos\alpha \end{pmatrix} \tag{5}$$

Hence, external the external variable that affects the linear acceleration in flight path direction $\ddot{x}_{wf}$ is the drag force D, while accelerations perpendicular to the flight path direction ($\ddot{y}_{wf}$ and $\ddot{z}_{wf}$) are affected by the lift force L.

Derivation of Rotational Acceleration around the Body Fixed Axes. The dynamic aircraft equations of motion (49) define the rotational acceleration acting around the aircraft's body fixed (bf) axes x_{bf}, y_{bf}, and z_{bf} such that

$$\dot{p} = \frac{P + I_{xz}\dot{r} - qr(I_{zz} - I_{yy}) + I_{xz}pq}{I_{xx}}$$

$$\dot{q} = \frac{Q - rq(I_{xx} - I_{zz}) - I_{xz}(p^2 - r^2)}{I_{yy}} \tag{6}$$

$$\dot{r} = \frac{R + I_{xz}\dot{p} - pq(I_{yy} - I_{xy}) - I_{xz}qr}{I_{zz}},$$

where $\dot{p}$ is the roll acceleration, $\dot{q}$ is the pitch acceleration, $\dot{r}$ is the yaw acceleration, p is the roll velocity, q is the pitch velocity, r is the yaw velocity, P is the roll moment, Q is the pitch moment, R is the yaw moment, and the elements of the moment of inertia tensor, such that (see Fig. S2)

$$I = \begin{bmatrix} I_{xx} & I_{xy} & I_{xz} \\ I_{yx} & I_{yy} & I_{yz} \\ I_{zx} & I_{zy} & I_{zz} \end{bmatrix}. \tag{7}$$

To estimate the effect of the external moments and the moment of inertia tensor on the LisHawk's agility in the respective aircraft fixed axis, the pure rotational motion is developed by assuming the rotational velocities of the other axes are zero, as stated in (8). Thus, Eq. 6 reduces to the variables which can directly be influenced by the morphing wing and tail (P, Q, R, and I), such that

$$\dot{\vec{\Omega}}_{pure} = \begin{pmatrix} \dfrac{P}{I_{xx}} \\ \dfrac{Q}{I_{yy}} \\ \dfrac{R}{I_{zz}} \end{pmatrix}. \tag{8}$$

The tail's effect on static pitch stability. The pitching stiffness is influenced by the location of the lifting surfaces, and can simplified (fuselage neglected, for small angles of attack) as

$$C_{m,\alpha} = -\frac{l_w}{\bar{c}_w} C_{Lw,\alpha} - \frac{S_t l_t}{S_w \bar{c}_w} \eta_t C_{Lt,\alpha}(1 - \epsilon_{d,\alpha}) \tag{10}$$

where $C_{Lw,\alpha}$ is the lift slope of the main wing, $C_{Lt,\alpha}$ is the lift slope of the tail, l_w is the distance between the center of gravity and the center of lift, l_t is the distance between the tail's center of lift and the center of gravity, S_w is the main wing's area, S_t is the area of the tail, $\bar{c}_w$ is the mean chord of the main wing, η_t is the efficiency of the tail dependent on the flow quality arriving the elevator, and $\epsilon_{d,\alpha}$ is the downwash angle of the flow arriving at the tail (8). Fig. S3 depicts the relations of the variables above in a schematic. To simplify Eq. 10, we assume $\eta_h = 1$ and $\epsilon_{d,\alpha} = 0$ so that

$$C_{m,\alpha} = -\frac{l_w}{\bar{c}_w} C_{Lw,\alpha} - \frac{S_t l_t}{S_w \bar{c}_w} C_{Lt,\alpha}. \tag{11}$$

The lift slopes, the wing planform areas, the distance l_t (aft tail configuration) and the mean aerodynamic chord are always positive. The change in l_t is small and it is hence assumed to be constant. From Eq. 11 it is accessible that the wing-tail combination is unconditionally stable if the center of gravity is in front of the center of lift, meaning that $l_w > 0$. For the LisHawk, shifting the wing into tucked wing increases l_w which increases longitudinal stability. A similar effect can be expected when the LisHawks tail area is increased. Contrarily, by sweeping the wing forward, l_w is reduced and can even become negative, hence becoming negative stable (unstable).

Flight Model Dynamics. A three degrees-of-freedom nonlinear flight dynamics model is used to describe the longitudinal motion of the feathered drone as expressed by the list of equations below (8, 44). The state variables V, α, γ, q, x and z correspond to the aircraft's velocity, angle of attack, flight path angle, pitch rate, horizontal and vertical displacements respectively. ρ refers to the density while g indicates the gravitational acceleration. m and S describe the mass and reference wing area of the aircraft respectively. M_y is the pitching moment about the aircraft's center of gravity and I_{yy} is the mass moment of inertia.

$$\dot{V} = \frac{T\cos\alpha - mg\sin\gamma - \frac{1}{2}\rho V^2 S C_D(\alpha, \delta_e, \delta_t, \delta_f)}{m} \tag{13}$$

$$\dot{\alpha} = q - \frac{T\sin\alpha - mg\cos\gamma + \frac{1}{2}\rho V^2 S C_L(\alpha, \delta_e, \delta_t, \delta_f)}{mV} \tag{14}$$

$$\dot{\gamma} = \frac{T\sin\alpha - mg\cos\gamma + \frac{1}{2}\rho V^2 S C_L(\alpha, \delta_e, \delta_t, \delta_f)}{mV} \tag{15}$$

$$\dot{q} = \frac{M_y(\alpha, \delta_e, \delta_t, \delta_f)}{I_{yy}(\delta_f)} \tag{16}$$

3

$$\dot{x} = V\cos\gamma \tag{17}$$

$$\dot{z} = -V\sin\gamma \tag{18}$$

In identifying the aircraft's optimum morphology for the lowest thrust requirement to sustain straight level flight condition (Fig. 6), the following zero-equality constraints are specified in the morphing shape optimization framework:

$$M_y\big(\alpha, \delta_e, \delta_t, \delta_f\big) = 0 \tag{19}$$

$$\frac{T\cos\alpha - mg\sin\gamma - \frac{1}{2}\rho V^2 S C_D\big(\alpha, \delta_e, \delta_t, \delta_f\big)}{m} = 0 \tag{20}$$

$$\frac{T\sin\alpha - mg\cos\gamma + \frac{1}{2}\rho V^2 S C_L\big(\alpha, \delta_e, \delta_t, \delta_f\big)}{mV} = 0 \tag{21}$$

$$\gamma = 0 \tag{22}$$

$$q = 0 \tag{23}$$

Aerodynamic Coefficients. Plots of lift coefficient (C_L), drag coefficient (C_D), pitching moment coefficient (C_m), rolling moment coefficient (C_l), and yawing moment coefficient (C_n) are based on the formulas from (5), which are shown below. L is the lift force in N, D is the drag force in N, Q is the pitching moment in Nm, P is the roll moment, R is the yawing moment, V is the velocity in m/s, S is the wing area in m^2, ρ is the air density in kg/m^3, c is the mean aerodynamic chord in m, and b is the wingspan in m (Fig. S2).

lift coefficient

$$C_L = \frac{2\,L}{\rho S V^2}$$

drag coefficient

$$C_D = \frac{2\,D}{\rho S V^2}$$

pitch coefficient

$$C_m = \frac{2Q}{\rho S c V^2}$$

Roll coefficient

$$C_l = \frac{2P}{\rho S b V^2}$$

yaw coefficient

$$C_n = \frac{2R}{\rho S b V^2}$$

Supplementary Figures
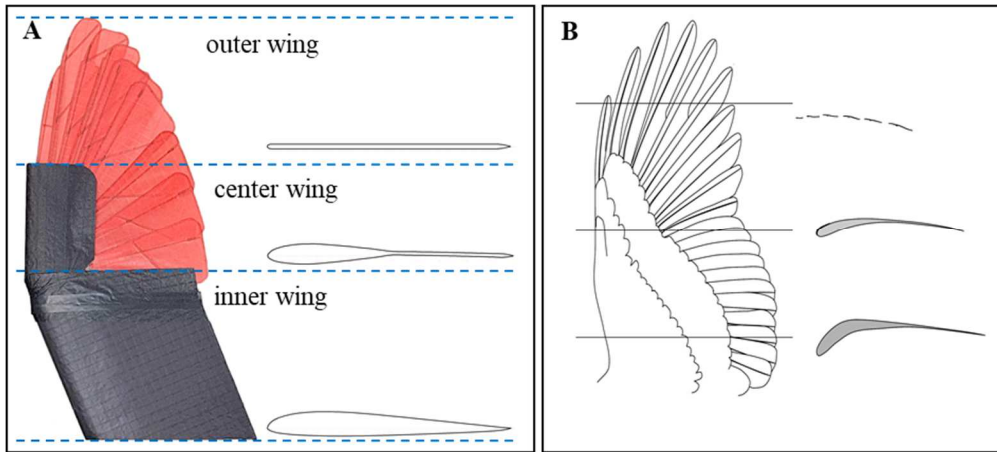
*Fig. S1. **Airfoil selection of the LisHawk compared to a bird's wing.** (**A**) The outer wing constitutes of overlapping artificial feathers which was modelled as a flat plate, for the center wing an adapted eagle profile is used, and for the inner wing the JWL-065 with a reflex trailing edge is considered. Airfoils presented are the ones used in the XFLR5 simulation process. (**B**) Undercambered airfoils and variable twist configuration of a bird's wing (56).*
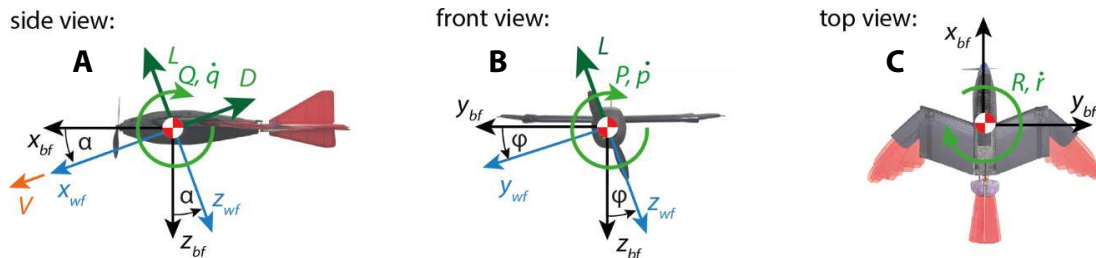
*Fig. S2. **Coordinate systems and variables used for describing the agility and maneuverability metrics used in this paper.** The red/white filled circle is the center of gravity. (**A**) Side view: Variables describing the side view are the x-axis in the body fixed frame x_{bf}, the z-axis in the body fixed frame z_{bf} (perpendicular to x_{bf}), the wind frame x-axis x_{wf}, the wind frame z-axis z_{wf} (perpendicular to x_{wf}), the angle of attack α, the flight velocity V, the lift L, the rag D, the pitching moment Q, and the pitching acceleration $\dot{q}$. (**B**) Front view: Variables describing the front view are the y-axis in the body fixed frame y_{bf} (perpendicular to x_{bf} and z_{bf}), the y-axis in the wind fixed frame y_{wf} (perpendicular to x_{wf} and z_{wf}), the bank angle φ, the roll moment P, and the roll acceleration $\dot{p}$. (**C**) Top view: Variables describing the top view are yawing moment R and the yawing acceleration $\dot{r}$. The sideslip angle is assumed to be small and hence the wind fixed axes are equal to the body fixed axes.*
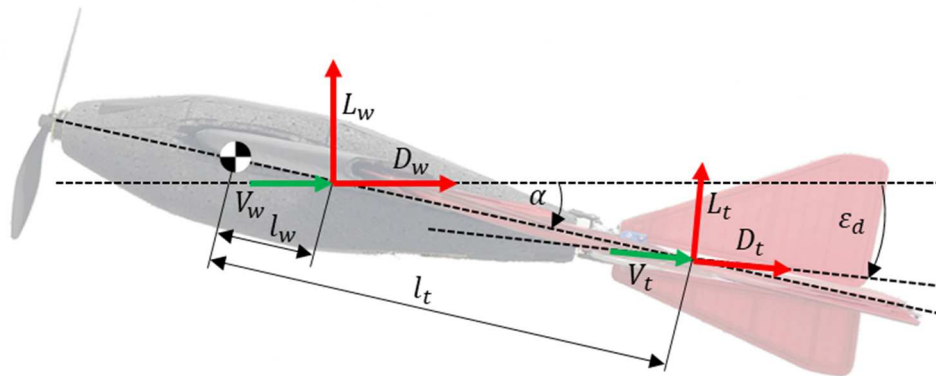
*Fig. S3. **Physical parameters that influence the pitch stability and their relation with the LisHawk platform.** Two lifting surfaces influencing the pitching stiffness can be distinguished: (i) The pitching moment caused by the main wing at a certain angle of attack α is influenced by the lift force L_w and the drag force D_w (perpendicular to L_w and parallel to the path velocity acting on the wing V_w) and the lever arm l_w. (ii) The tail's contribution is a function of the tail's lever arm l_t, the tail's lift L_t and the tail's drag D_t. The drag force is again parallel to the incoming airflow V_t, which is different from α due to the downwash generated by the main wing.*
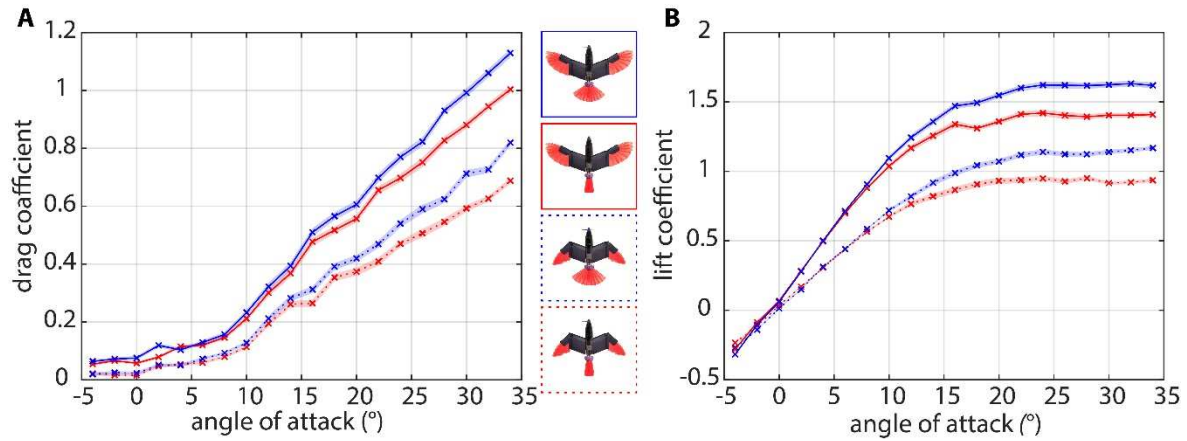
Fig. S4. **Standard deviation and measured points of the lift and drag plots.** *The shaded areas indicate the standard deviation and the markers (x) indicate the measured pints. (A) Drag coefficient with respect to the angle of attack, as seen in Fig. 3B to D. (B) Lift coefficient with respect to the angle of attack, as seen in Fig. 3B to D.*
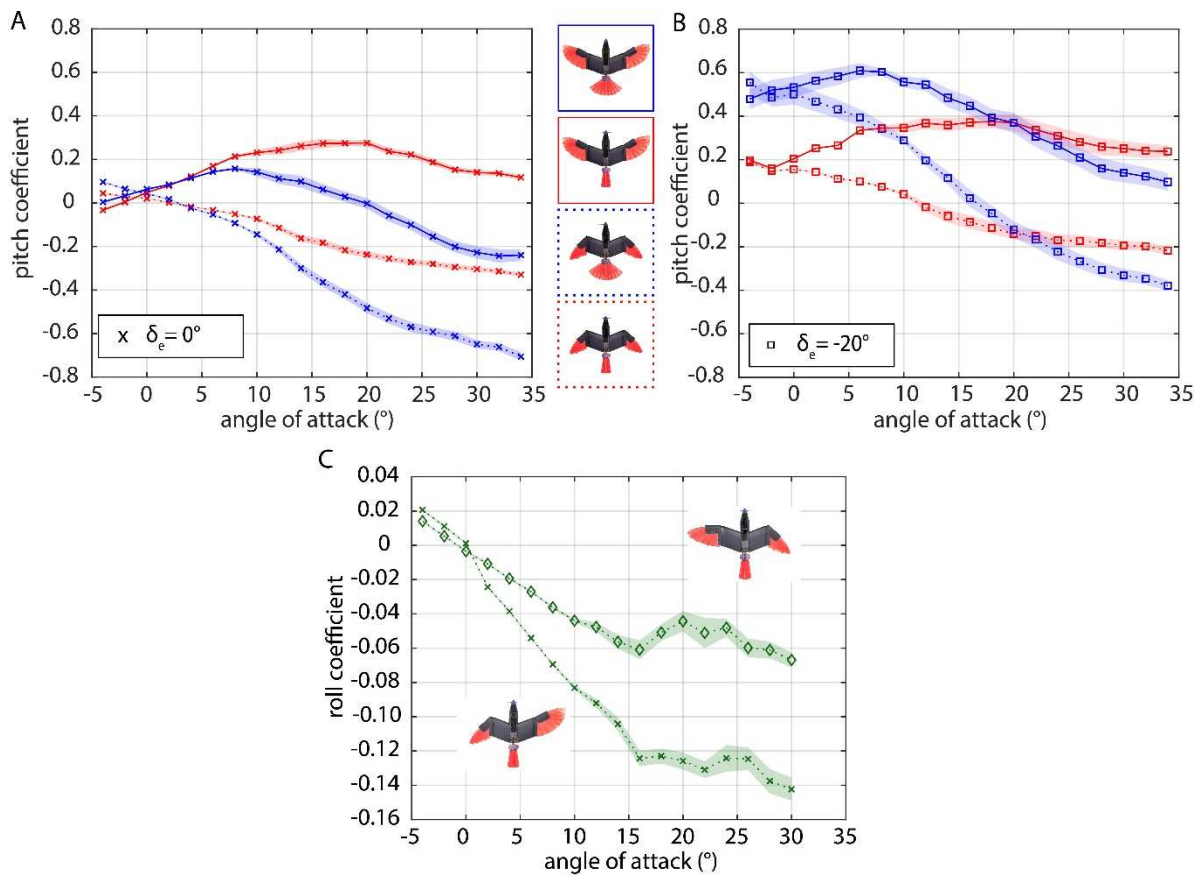
Fig. S5. **Standard deviation and measured points of the pitch moment and roll moment plots.** *The shaded areas indicate the standard deviation and the markers indicate the measured pints for an elevator deflection δ_e of 0° (x) and -20° (square). (A) Pitch coefficient with respect to the angle of attack, as seen in Fig. 5B to D. (B) Pitch coefficient resulting from an elevator deflection (-20°, upward) with respect to the angle of attack, as seen in Fig. 4A to D. (C) Roll coefficient resulting from two different asymmetric wing sweep angles (45° and 85°) with respect to the angle of attack, as seen in Fig. 4F.*

Supplementary Movies

Mov. S1. Morphing wing fabrication. This movie shows each assembly step of the wing morphing mechanism and provides information on the materials used.

Mov. S2. Morphing tail fabrication. This movie shows the assembly steps of the tail mechanism and the materials used.

Mov. S3. Morphing control surfaces. This movie shows the LisHawk's morphing capabilities.

Mov. S4. Flight test. This video shows the LisHawk in flight in different morphing configurations and flight regimes and its behaviour during aggressive and cruising flight.

Mov. S5. Pull up maneuver. Pull up maneuver for all three cases of tucked wing and tail, tucked wing and extended tail, and extended wing and tail to show increased agility and maneuverability due to morphing.